Multiscale Modeling of the Effects of Unlimited Four-Membered Ring Formation on Sol-Gel Silica Film Molecular Structure

Xin Li and Stephen E. Rankin
Dept. of Chemical and Materials Engineering, University of Kentucky, Lexington, KY 40506

DOI 10.1002/aic.13853
Published online June 15, 2012 in Wiley Online Library (wileyonlinelibrary.com).

A modified multiscale model of a sol-gel silica drying process is presented that treats first-shell substitution effects and unlimited four-membered ring cyclization. The inclusion of four-membered (8-atom) rings allows the model to simulate the formation of the tetrasiloxane rings and cubic silsesquioxane cages known to be prevalent components of sol-gel silica systems, as well as a full range of other ring-containing structures. The polymerization process is treated using a dynamic Monte Carlo method where a discrete population of one million monomers evolves according to kinetic rules, including unimolecular-like closure of three-bond blocks. Compared with prior simulations with extensive cyclization that allowed only three-membered rings, the molecular structures formed with unlimited four-membered ring are more complex, and the occurrence of ''skinning'' (the rapid formation of a gel only at the surface of the film) is more pronounced and leads to more severe structure gradients. © 2012 American Institute of Chemical Engineers *AIChE J,* 59: 707–718, 2013
Keywords: multiscale modeling, sol-gel silica, film, dynamic Monte Carlo, polycondensation, four-membered rings

Introduction

Sol-gel silica films and related polycondensation networks are of growing interest in industrial practice and as sources of novel materials.[1] In particular, there has been an explosive growth in the design of mesoporous and macroporous silica-based thin films in the last two decades, which is based on the formation of a silica gel near ambient conditions in the presence of a structure-directing agent.[1–4] The process of forming sol-gel silica films by dip coating couples polymerization and drying, i.e., it involves multiple length and time scales ranging from molecular to macroscopic.[5–9] Therefore, a multiscale model is necessary to link different length and time scales together throughout the entire simulated domain.[10,11]

At the molecular scale of the sol-gel silica polymerization process, cyclization occurs as a nonrandom, preferential reaction[12–14] and delays gelation to a siloxane bond conversion of about 82%[15–17] (this value can be compared to a value of 33% expected for random, ideal polycondensation[18]). Large concentrations of three- and four-membered ring containing species have also been found during sol-gel silica polymerization by theoretical and analytical techniques including quantum chemical calculations,[12,19] ^{29}Si NMR,[14,16,20–24] vibrational spectroscopy,[25,26] X-ray/neutron scattering,[13,27,28] and gas chromatography.[13,29] Therefore, cyclization should be taken into account in the polymerization process modeling. We recently added unlimited three-membered ring cyclization into our multiscale dynamic Monte Carlo (DMC)/continuum model as our first step to investigate the effects of cyclization on the sol-gel silica film coating process. However, experiments show that four-membered rings dominate over and are more stable structural units than three-membered rings in real silicates.[19,25–28] A number of recent off-lattice simulations of silica polycondensation based on classical or density functional theory-derived potentials also indicate that four-membered rings are significantly more important than three-membered rings.[30–34] A polymerization model allowing the formation of four-membered rings should give better qualitative and quantitative predictions than those allowing only intermolecular reactions (even with substitution effects) or only three-membered rings. Based on our previous work with a model allowing unlimited formation of three-membered rings, we will describe a modified multiscale model with unlimited four-membered ring formation. While it seems to be a simple extension of the three-membered ring polymerization model, accounting for all possible types of 3-bond blocks and their evolution during polymerization introduced structural modeling challenges that needed to be addressed. Most importantly, the approach presented here brings the prediction of cyclization by DMC methods into a physically reasonable concentration range for the first time.

In our multiscale model, the entire DMC simulation is treated as a particle of sol whose position and composition are tracked in a continuum model. A nonspatial population balance DMC method is used to permit a large number of monomers to be simulated, which is essential for predictions

Correspondence concerning this article should be addressed to S. E. Rankin at srankin@engr.uky.edu.
Current Address of Xin Li: Huntsville, AL.

close to the gel point.[35,36] Simulations in three-dimensional space allow effects such as diffusion and cyclization to emerge naturally from the intermolecular and intramolecular potentials, respectively, but limit the system size to a few thousand monomers.[31,32,34] Linking the two models is accomplished by synchronizing time steps and concentrations between the continuum and DMC models while tracking the positions of sol particles during drying. This approach is required because the polymerization and drying processes occur throughout the sample volume rather than occurring in domains that are relatively easy to separate (as in catalysis,[37] thin film deposition,[38–41] and etching[42]). The DMC/continuum multiscale modeling approach allows us to observe the competition between growth and cyclization, and between drying and gelation. The quantitative predictions of the new four-membered ring calculations are compared with those based only on three-membered rings to show the likely impact of ring size on the severity of phenomena such as gelation delay, skinning, and structure gradients in drying sol-gel silica films.

DMC Model

Bimolecular condensation

The DMC model of silica sol-gel polymerization is designed with kinetic trends observed under acidic conditions where homogeneous silica gels can be produced (pH 2–4). Experiments have shown that under acid-catalyzed conditions, for alkoxysilane solutions, hydrolysis reaches pseudoequilibrium.[23,43,44] This equilibrium condition allows one to characterize hydrolysis using only the average hydrolysis extent χ[45]

$$\chi = \frac{[\mathrm{SiOH}]}{[\mathrm{SiOH}] + [\mathrm{SiOR}]} \tag{1}$$

Where SiOH denotes a hydroxyl functional group, SiOR denotes an alkoxyl functional group (R = an alkyl group such as ethyl or methyl), and square brackets denote concentrations. Because hydrolysis equilibrium coefficients are all similar regardless of substitution, it is possible to regard χ as a constant for all silicon sites.[44] Also, we assume that the amount of water is sufficient that χ can be regarded as constant with respect to time as well.[43]

Based on previous kinetic studies, we assume that water-producing condensation dominates over alcohol-producing condensation,[46,47] and that a strong, negative first shell substitution effect (FSSE) is operative for the condensation reactions.[43,48] The FSSE arises because of steric hindrance near the site of a condensation reaction, and therefore is thought to be negative. With these assumptions, the set of bimolecular condensation can be simplified to[49]

$$Q_i + Q_j \xrightarrow{k_{ij}} Q_{i+1} + Q_{j+1} + \mathrm{H_2O} \quad i,j = 0,1,2,3 \tag{2}$$

where Q_i represents a tetrafunctional silicon site with i siloxane bonds. Thus, the rate expressions for bimolecular reactions between silicon sites are[49]

$$R_{ij}^{bimol} = \begin{cases} k_{ij}^*(f-i)(f-j)[Q_i][Q_j], & i \neq j \\ \frac{1}{2}k_{ij}^*(f-1)(f-j)[Q_i][Q_j], & i = j \end{cases} \tag{3}$$

where $k_{ij}^* = \chi^2 k_{ij}$, k_{ij} is the rate constant of bimolecular polycondensation and f is the functionality of the monomer ($f = 4$ for tetrafunctional silane precursors). The rate coefficients are set according to the experimental trend[50]

$$K^* = k_{00}^* \begin{bmatrix} 1.0 & 0.9 & 0.81 & 0.729 \\ & 0.1 & 0.09 & 0.081 \\ & & 0.01 & 0.009 \\ & & & 0.001 \end{bmatrix}$$

Cyclization

A cyclization reaction occurs when the two sites chosen to react are in the same molecule. This intramolecular reaction causes a new ring to form. Usually in DMC simulations, if the sites chosen to react by a bimolecular reaction are members of the same molecule, they are not allowed to react. This prevents unrealistic random intramolecular reactions from occurring at a rate that does not take into account the bonding restrictions that favor certain sizes of rings. Similar to our previous work[11] regarding three-membered rings, we use bond blocks ${}^nB_{ij}$ to explicitly calculate cyclization rates based on quasi-unimolecular reactions of these structural units. Here the superscript n represents the number of siloxane (Si—O—Si) bonds linking one site to another, and the subscripts i and j represent the connectivities of the sites at the ends of the block (i.e. the numbers of siloxane bonds attached to each end). Since four-membered rings are prevalent and more stable than three-membered rings in real silicates, we model cyclization reactions to form only four-membered rings. Therefore, we just need to pay attention to three-bond blocks. Based on this approach, the rates of cyclization reactions are calculated according to the following expression[49]

$${}^4R_{ij}^{\mathrm{cyc}} = (f-i)(f-j)k_{4c(i,j)}^*[{}^3B_{ij}], \quad i\,j = 1,2,3 \tag{4}$$

We assume that the substitution effect for cyclization reactions follows the same trend as for bimolecular reactions, since it still involves nucleophilic displacement between sites of varying connectivity

$$K_{4c}^* = k_{4c(1,1)}^* \begin{bmatrix} 1.0 & 0.9 & 0.81 \\ & 0.1 & 0.09 \\ & & 0.01 \end{bmatrix}$$

To characterize the cyclization tendency, the dimensionless parameter κ is used as defined by Rankin et al.[49]

$$\kappa \equiv \frac{k_{4c(1,1)}^*}{k_{11}^*[\mathrm{Si}]_0} \tag{5}$$

where $[\mathrm{Si}]_0$ is the initial monomer concentration.

Monte Carlo algorithm

The DMC simulation procedures are the same as our previous model with three-membered ring cyclization[11] with the exception of the bond blocks modeled. DMC simulation methods have been widely utilized since they were introduced by Gillespie[51] and their use in wide-ranging fields has been recently reviewed.[52,53] Our DMC simulation starts from a finite set of N monomers (which is equal to 10^6 in our model). The condensation reaction conversion in the simulation, α, is defined as the number of siloxane bonds added relative to the total number possible (this will sometimes be referred to as simply the "conversion" because it is the

primary reaction of interest). Because each monomer is tetrafunctional in silicates, α can be calculated by dividing the number of bonds added by $2N$ (the maximum number of bonds that can be added between N tetrafunctional monomers). At each DMC step, a new siloxane bond is formed, and the conversion is increased by a small constant value (which is $1/2N = 5 \times 10^{-7}$ here).

As in all continuous-time DMC methods, a reaction occurs at every step but the probability of selecting a particular reaction type is proportional to its rate.[51,52,54] The probabilities are normalized by dividing the rate of each bimolecular or cyclization reaction by the sum of the rates of *all* bimolecular and cyclization reactions, and the reaction is selected by first ordering the probabilities along a scale from 0 to 1 and using a random number generator to make the choice. If a bimolecular reaction is chosen, the sites that react are each randomly selected from the list of all sites with the appropriate connectivities. If cyclization is chosen, we randomly select one three-bond block with the appropriate end connectivities from the corresponding linked list of bond blocks (see later). Then we update all data structures including the bonded neighbor lists for the participating sites, three-bond block lists, molecular weight, Wiener index (see later), cycle rank, and so on. Supporting Information Table S1 lists the data structures used to track the polymerization. We also track the number- and weight-average degrees of polymerization (DP_w and DP_n), number-average Wiener index (W_n), number-average (Cr_n) and weight-average (Cr_w) cycle rank of the whole population as defined below.

The time interval is given by the expression originally derived by Gillespie[51,54]

$$\Delta t = \frac{C_{Si}}{N \sum (R_{ij}^{bimol} + {}^4R_{ij}^{cyc})} \ln\left(1/r\right) \tag{6}$$

where N is the total number of sites, r is a random number selected from the interval (0, 1), and R_{ij}^{bimol} and ${}^4R_{ij}^{\mathrm{cyc}}$ are the rates given by Eqs. 3 and 4. In this expression, C_{Si} is the total silicon site concentration which comes from the continuum model results at the moment that the reaction is selected. This concentration serves as one link between the DMC model and the continuum model in this multiscale modeling strategy. Once a particular reaction has been chosen, sites are randomly selected from among the populations that match the reactants (connectivity and, if a cyclization reaction, bond block membership). In the simulation, all monomers have unique indices assigned at the beginning of the simulation, and data structures summarized in Supporting Information Table S1 are used to maintain information about the system. The site indices are used to keep track of the bonding between monomers, from which all information about molecular structure is derived, including bond block concentrations. The largest differences between the models with three- and four-membered rings are involved with updating the Wiener index after a cyclization reaction and maintaining the lists of bond blocks (for three-bond blocks rather than two-bond blocks).

The Wiener index[55] is a topological index that can be directly related to molecular compactness and rheology of suspensions.[56] It is defined to be the sum of the topological distances (the minimum number of siloxane bonds connecting two silicon atoms) between all sites in a molecule. Updating the Wiener index of a molecule after a bimolecular reaction was described in our previous paper with unlimited

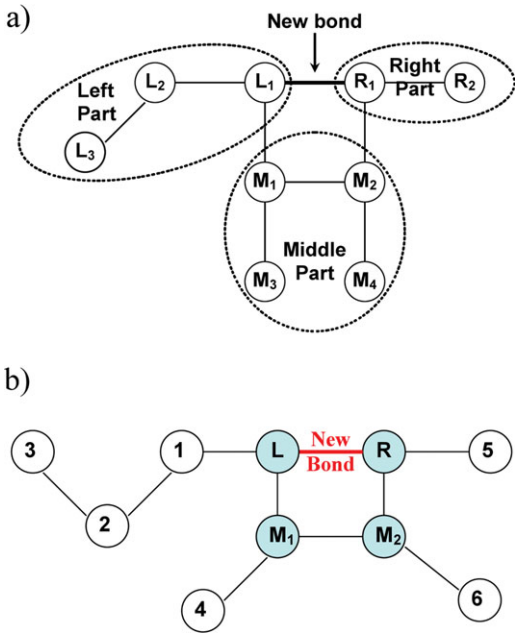

Figure 1. Schematic diagrams of the product of a cyclization reaction producing a four-membered ring. Circles represent silicon sites and lines represent siloxane bonds.

The sections of the figure illustrate (a) dashed circles identifying the left, middle, and right fragments of a molecule and (b) a specific example used to illustrate how 3-bond blocks are updated due to a cyclization reaction. [Color figure can be viewed in the online issue, which is available at wileyonlinelibrary.com.]

three-membered ring cyclization.[11] We use a similar procedure here; when a bimolecular reaction occurs, the reacting molecules are traversed using neighbor lists that are updated as bonds are added. If the molecules react due to a bimolecular reaction between site L (part of a molecule of size n) and site R (part of a molecule of size m), then the change in the Wiener index of the molecule is given by W_{new}, which is the contribution that comes about due to the new siloxane bond[11]

$$W_{new} = n \sum_{i=1}^{m} d_{iR} + m \sum_{j=1}^{n} d_{Lj} - mn \tag{7}$$

where $d_{i,j}$ is the topological distance between site i and site j in one of the two reacting molecules, which is found by counting bonds while traversing the sites of the molecule. To update the Wiener index of a molecule due to a four-membered ring cyclization reaction, we separate the whole molecule into three parts: left part, middle part and right part as shown in Figure 1a.

Because the new ring has four members (rather than three), the distance from each site in the left part (of size m) to each site in the right part (of size n) is decreased by 2 after cyclization. At the same time, the distance from each site in the middle part of the molecule to each site in the left and right parts remains unchanged. Therefore, if we know the sizes of the left and right parts, the calculation of the change in the Wiener index, W_{new}, is very simple

$$W_{\mathrm{new}} = -2mn \tag{8}$$

Therefore, the Wiener index of the molecule after cyclization is

$$W = W + W_{\text{new}} = W - 2mn \tag{9}$$

For example, in Figure 1a, the left part has three nodes, the middle part has four nodes and the right part has two nodes. After the cyclization reaction, the Wiener index decreases by 12. For the general case in our DMC program, we traverse both the left and right parts of a molecule (using a matrix of the neighbors bound to each site) to calculate the number of sites (the size) of each part.

To maintain the necessary information about three-bond blocks, we use six linked lists to record all three-bond blocks capable of forming rings, sorted by connectivity of their ends. To have the concentrations of these three-bond blocks, information about ${}^3B_{ij}$ needs to be updated after each reaction step by adding newly created bond blocks created and modifying old ones changed by the reaction. This is done using an algorithm that was written to first count all possible new 3-bond blocks formed due to the new bond (moving outward in shells of nearest neighbors starting from the reacting sites L and R) and then carefully checking to avoid redundancy and the possibility that 3 bonds is not actually the shortest topological distance between possible new bond blocks. Figure 1b shows an example. When a new bond is formed between site L and R in a cyclization reaction, six new 3-bond blocks need to be added, which are L-R-M_2-6, R-L-1-2, R-L-M_1-4, 1-L-R-5, 1-L-R-M_2, and M_1-L-R-5. At the same time, three old 3-bond blocks need to be modified, L-1-2-3, L-M_1-M_2-6, and R-M_2-M_1-4, because the connectivities of L and R are both changed from 2 to 3. Besides that, the 3-bond block L-M_1-M_2-R that forms a cycle needs to be deleted.

Once the four-membered cyclization reaction rates are calculated based on the concentration of all 3-bond blocks, Monte Carlo reaction selection can be performed at each step to choose one reaction to occur. As noted above, one reaction occurs at each Monte Carlo step, and is selected using probabilities proportional to the rates of the reactions. The set of data structures that is maintained to accomplish this is outlined in Supporting Information Table S1. Averaged quantities are also calculated to provide insight into the collective behavior of the system. Several number- and weight- averaged quantities are defined as follows: where degree of polymerization (DP) refers to the number of sites in a molecule, cycle rank (Cr) refers to the number of unique cyclic structures in a molecule (equivalent to the minimum number of bonds that must be broken to remove all cycles from the polymer structure), and Wiener index (W) is defined above.

$$DP_n = \frac{\sum_{i=1}^{N_{\text{mol}}} DP_i}{N_{\text{mol}}} = \frac{N}{N_{\text{mol}}} \text{ and } DP_w = \frac{\sum_{i=1}^{N_{\text{mol}}} (DP_i)^2}{\sum_{i=1}^{N_{\text{mol}}} DP_i} = \frac{\sum_{i=1}^{N_{\text{mol}}} (DP_i)^2}{N} \tag{10}$$

$$W_n = \sum_{i=1}^{N_{\text{mol}}} W_i \cdot \frac{1}{N_{\text{mol}}}, Cr_n = \sum_{i=1}^{N_{\text{mol}}} Cr_i \cdot \frac{1}{N_{\text{mol}}} \text{ and } Cr_w = \frac{\sum_{i=1}^{N_{\text{mol}}} Cr_i \cdot DP_i}{N} \tag{11}$$

where N_{mol} is the total number of molecules, W_i is the Wiener index of molecule i, Cr_i is the cycle rank of molecule i, and DP_i is the degree of polymerization of molecule i. These averaged quantities could be recalculated periodically based on the distributions of molecules with different degrees of polymerization, Wiener indices, and cycle ranks, but in Supporting Information Table S2 we present formulas that were used to update each of these quantities after a single Monte Carlo step.

Using the DMC approach, we are able to explicitly track all information about three-bond blocks formed and consumed in the course of polymerization, and then to use this information to calculate the cyclization rates. This is the advantage of the DMC method compared with statistical models, which assume that bond block populations can be derived from the populations of constituent sites. Even the hybrid Monte Carlo/spanning-tree model of Sarmoria and Miller used the Monte Carlo method to sample the populations of bond blocks about a given site based on randomly joining sites according to the polymerization conversion.[57] This approach is likely to introduce systematic errors for highly nonrandom polymerization such as the polymerization we are modeling here. Another advantage of the DMC approach is that we can obtain structural parameters including the gel point, molecular weight distribution, Wiener index, etc., which are related to film microstructure and are not readily available from a continuum kinetic model.

Continuum drying model

The one-dimensional continuum transport model for the formation of sol-gel thin-film coatings is exactly the same as the one described in our previous multiscale modeling work.[10] Please refer to our previous paper for a more detailed discussion of the assumptions and modeling equations, which are briefly discussed here. For the present study, we assume that alcohol (ethanol) is the sole solvent. A schematic diagram of the sol-gel film drying process is given in Supporting Information Figure S1.

Governing Equations. Since the validity of our multiscale model has been verified using cases where differential equations for the evolutions could be explicitly written (i.e., without cyclization),[10] we can simplify the continuum model to consider the transport of only solvent and total silica, without balance equations for individual Q_i reactant species. Therefore, assuming only diffusion inside of the film, the governing equations are simply written as follows

$$\frac{\partial C_1}{\partial t} - D_1 \frac{\partial^2 C_1}{\partial z^2} = 0 \tag{12}$$

$$\frac{\partial C_2}{\partial t} - D_2 \frac{\partial^2 C_2}{\partial z^2} = 0 \tag{13}$$

where C_1 is the concentration of solvent, C_2 is the total silicon concentration, and D_i is the diffusion coefficient for each species.

Initial conditions in this formulation are as follows

$$C_1(0, z) = C_{1,0}; \quad C_2(0, z) = C_{2,0} \tag{14}$$

Consistent with the description of the film model represented in Supporting Information Figure S1, the boundary conditions are given by

$$\text{At the substrate } (z=0): D_i \frac{\partial C_i}{\partial z} = 0 \ (i=1,2) \tag{15}$$

$$\text{At the free surface } (z=H(t)): -D_1 \frac{\partial C_1}{\partial z} - C_1 \frac{dH(t)}{dt} = k_g(y_1^s - y_1^\infty) \tag{16}$$

$$\frac{\partial C_2}{\partial z} = -\frac{\hat{V}_1}{\hat{V}_2}\frac{\partial C_1}{\partial z} \tag{17}$$

The effect of boundary motion due to solvent evaporation is taken into account using the term $\frac{dH(t)}{dt}$.[58] In Eq. 16, k_g is the mass-transfer coefficient of solvent in the vapor-phase, y_1^s is the molar fraction of solvent just above the film surface in the gas phase (which is calculated based on Raoult's law), and y_1^∞ is the molar fraction of solvent in the gas phase far away from the film, which is set to zero here. Equation 17 was derived from the relation $C_1\hat{V}_1 + C_2\hat{V}_2 = 1$, where $\hat{V}_i$ is the molar volume of species i, and $\hat{V}_2 = \frac{1-C_{1,0}\hat{V}_1}{C_{2,0}}$. Because only solvent is assumed to evaporate, the rate of change of film thickness, also known as the surface velocity v^s, can be calculated according to the following expression

$$\frac{dH(t)}{dt} = v^s = -\hat{V}_1 k_g(y_1^s - y_1^\infty) \tag{18}$$

Dimensionless Variables and Simulation Procedure. The following dimensionless variables are defined to solve the transport equations numerically

$$\eta = z/H(t), \quad h = H(t)/H_0, \quad c_i = C_i/C_{2,0}, \quad \tau = \frac{D_1}{H^2}t \tag{19}$$

Using the dimensionless variableη, the region in which diffusion occurs ranges from $\eta = 0$ to $\eta = 1$. In other words, the physical moving domain is mapped onto a fixed domain, and we do not need to modify the spatial grid during the simulation. Meanwhile, a pseudoconvective term is produced by this Landau transformation[59] in the diffusion equation.[58] For example, the dimensionless form of the equation for the solvent now is

$$\frac{\partial c_1}{\partial \tau} - \frac{\eta}{h}\cdot\frac{dh}{d\tau}\cdot\frac{\partial c_1}{\partial \eta} - \frac{1}{h^2}\cdot\frac{\partial^2 c_1}{\partial \eta^2} = 0 \tag{20}$$

We can see that this pseudoconvective term is proportional to the free surface velocity $\frac{dh}{d\tau}$.

This set of dimensionless equations is numerically solved using explicit centered finite difference method (FDM). We discretize the whole domain into a number of thin slices; each one has a fixed thickness $\Delta\eta$. For the solution, the time interval Δt is equal to the time interval between reactions estimated from the DMC simulation. As mentioned above, this time interval from the DMC model serves as one "handshake" with the continuum model. At each finite difference step, we use the concentrations, film thickness, the surface velocity, and Robin boundary condition at the surface from the previous time step to complete the calculation. The entire DMC simulation is treated as a particle of sol whose position and composition are tracked in the continuum model. The particle tracking is based on the net diffusion of solvent at the current position of the particle, and can be expressed by the following equation

$$\frac{dH_p(t)}{dt} = \hat{V}_1 \cdot D_1 \frac{\partial C_1}{\partial z}\bigg|_{H_p} \tag{21}$$

Equation 21 is implemented by nondimensionalizing the equation using the same approach as for Eq. 20 and solving by the centered finite difference method to provide $h_p = H_p(t)/H(t)$. The concentration within the sol particle is estimated by linear interpolation using the closest two grid points, and the total silicon site concentration is supplied to the DMC routine to choose the next reaction and calculate the time interval of the next DMC step, as discussed previously.[10]

Parameters. In our modeling, we focus on the effects of three important dimensionless parameters to understand how process parameters affect the drying process of the sol-gel silica film. In addition to the dimensionless cyclization tendency κ mentioned earlier, the other two are *Bi* and *Da* (Eq. 22). *Bi* is the Biot number, which is the ratio of external mass-transfer resistance to the internal diffusion resistance, and can be thought of as a dimensionless mass-transfer time. *Da* is the Damköhler number, which is the ratio of reaction rate to diffusion rate, and can be thought of as a dimensionless reaction time. We use the first reaction rate coefficient k_{00}^*as the reference to define the Damköhler number because one (of several) rate coefficient is required to define a constant dimensionless number. For a negative FSSE (considered here) $k_{00}^*$is the largest rate coefficient.

$$Bi = \frac{k_g H_0 \hat{V}_1}{D_1}, \quad Da = \frac{k_{00}^* C_{2,0} H_0^2}{D_1} \tag{22}$$

The values of parameters D_1,$\hat{V}_1$,k_g, and so on are set to arbitrary values in the model, because these values are not easy to obtain and they may change during drying and gelation; in addition, the dimensionless form of our model makes it insensitive to specific values of parameters, and allows us to focus on the competition between the drying and gelation process, and how this competition affects the coating structure. Still, it should be possible to relate a good model to real process parameters; in the future it should be possible to use structure-property relationships based on the Wiener index to even handle changing transport coefficients during coating. For now, we use constant values in our program, which are given by $C_{1,0}:C_{2,0} = 4:1$, $C_{2,0} = 1.0$ mol/L, $\hat{V}_1 = 0.1\text{cm}^3/\text{mol}$, and $D_1 = D_2$.

Results and Discussion

As in our previous paper about forming three-membered rings,[11] we will present the results of forming four-membered rings in terms of conversion, number-average Wiener index, cycle rank, ring involvement, gelation regime map and structure gradient map. Some of these results will be compared with the results of a model allowing only three-membered rings.

Conversion at gelation

Figure 2 shows the weight-average degree of polymerization (DP_w) calculated by the model with four-membered rings as a function of siloxane bond conversion (α) for a specific set of drying conditions, for varying values of κ. The divergence of the curve indicates the point of gelation. Simulations were run until this criterion for gelation was

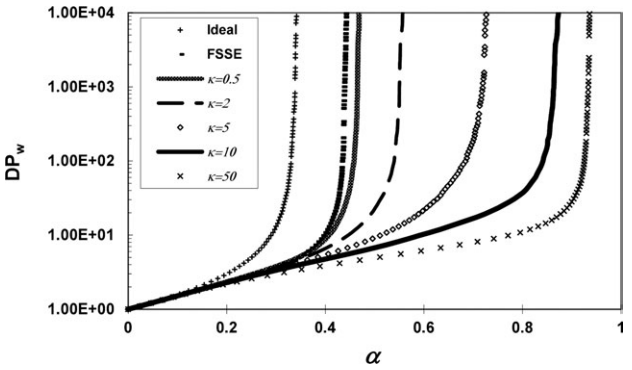

Figure 2. Weight-average degree of polymerization from DMC model with unlimited four-membered rings as a function of siloxane bond conversion for varying κ with $Bi = 1000$, $Da = 60$, and $h_{p0} = 0.8$.

observed and the films were completely dry (indicated by the point at which $C_1 = 0.01C_{1,0}$) Similar with the results of a model with unlimited three-membered rings,[49] the gel conversion increases as cyclization tendency κ increases. It is clear from Figure 2 that cyclization delays gelation, and that for some values of κ, the gel conversion can be as large as or larger than the experimental value for tetraalkoxysilanes (82%).[15–17]

The gel conversions as a function of dimensionless cyclization tendency κ for models with three- or four-membered rings are also compared in Figure 3. There are no qualitative differences of gel conversions between simulations with the two types of rings. The curves can be divided into several parts: when $\kappa \leq 0.5$ or $\kappa \geq 20$, gel conversions are almost constant with respect to κ for both cases. When $1 \leq \kappa \leq 3.5$, gel conversions with three-membered rings are a little larger than with four-membered rings. When $5 \leq \kappa \leq 20$, on the contrary, gel conversions of four-membered rings cyclization are a little larger than those of three-membered rings cyclization. This transition from the range of κ giving almost no cyclization ($\kappa \leq 0.5$) to the range of κ giving cage-like precursor formation before gelation ($\kappa \geq 20$) occurs over a narrower range in the model with four-membered rings. However, the assumptions behind the model with four-membered rings are more realistic. Experiments have shown that three-membered ring formation is reversible, at least in the case of methyl-modified precursors,[23]

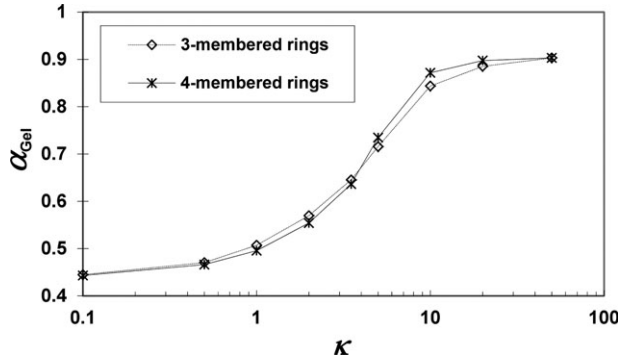

Figure 3. Gel conversion (α_{gel}) as a function of cyclization tendency κ with $Bi = 1000$, $Da = 60$, and $h_{p0} = 0.8$.All points are the average values from five repeated calculations.

Table 1. Counts of Total, Bimolecular, and Cyclization Reaction Steps in DMC Simulations with Three- or Four-Membered Rings

$\kappa = 50$	Three-Membered Ring Cyclization	Four-Membered Ring Cyclization
S_b	909,386	949,028
S_c	957,013	919,864
S_t	1,866,399	1,868,892

Here, $Bi = 1000$, $Da = 60$, $hp_0 = 0.8$.

which has not been accounted for in our model (but which would presumably cause lower conversions at gelation with three-membered rings). Also, the experimental value of κ is about twice as large for four-membered rings as for three-membered rings,[22] which would favor the high conversions at gelation observed experimentally.

As we mentioned before, at each MC step, a new siloxane bond is formed, and the conversion is increased by a small constant value (which is 5×10^{-7} in our model). So in fact, the gel conversion is determined by the total number of MC steps required to reach the gel point. We can divide the total MC steps into two parts

$$S_t = S_b + S_c \tag{23}$$

where S_t is the total number of MC steps at the gel point, S_b is the number of bimolecular reactions steps and S_c is the number of cyclization reactions. At each bimolecular reaction step, the total number of molecules decreases by one, while at each cyclization reaction step, the total number of molecules remains the same. We keep track of the numbers of reaction steps for $\kappa = 50$ and show the results in Table 1. This table shows that more bimolecular reactions occur in the four-membered ring case (50.7%) than with three-membered rings (48.7%). This suggests that at gelation, the total number of molecules in the four-membered ring system is smaller than in the three-membered ring system. The net result (as we will discuss later) is a higher number-average cycle rank with four-membered rings. This is not surprising given that more bonds must form before cyclization can begin in this case, but it is still a cause for much of the structural complexity to be discussed below.

Wiener index

The Wiener index can be used as a measure of molecular compactness. Figure 4 shows the scaled Wiener index ($W_n/W_{n,lin}$) as a function of conversion for varying κ in the DMC simulations. All of the curves start from 1 and decrease with increasing conversion. That means the molecules are becoming more compact than linear molecules of comparable degree of polymerization would be. This is due to branching and cyclization (for $\kappa \neq 0$). Since a negative FSSE results in polymers that are more linear than in the ideal polycondensation case, the scaled Wiener index is larger at a given conversion for FSSE ($\kappa = 0$) and cyclization (for $\kappa \neq 0$) compared with ideal polycondensation. Figure 4 also clearly shows that cyclization delays the gelation. The only exception is when $\alpha < 0.2$ with $\kappa = 50$. In this region, the value of the scaled Wiener index with $\kappa = 50$ is identical to or larger than that of the ideal case for four-membered ring cyclization, while the opposite was observed for three-membered rings.[11] This is because 3-bond blocks are formed later than 2-bond blocks, so four-membered ring cyclization reactions start later and occur less in the beginning of the polycondensation process than for three-membered rings. For

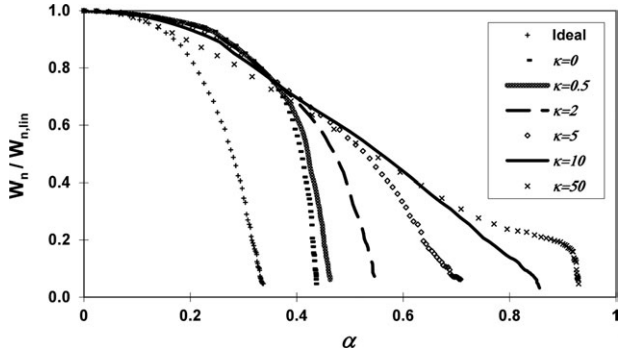

Figure 4. Evolution of $W_n/W_{n,lin}$ as a function of siloxane bond conversion for varying κ in DMC simulations of polycondensation with four-membered rings: *Bi* = 1000, *Da* = 60, h_{p0} = 0.8.

$\alpha < 0.15$, it is also possible that the compaction effect of four-membered ring cyclization can offset the effects of negative FSSE for molecular growth. Therefore, the curve of $\kappa = 50$ appears similar to the ideal case for $\alpha < 0.15$.

Cycle rank

The cycle rank of an oligomer represents the number of independent cycles that must be closed to form that structure.[49] Supporting Information Figure S2 shows the number-average cycle rank for simulations with four-membered rings and various κ values as a function of DP_w. This figure shows similar trends to what was observed for three-membered ring cyclization.[11] The development of cyclization can be divided into three stages. Little cyclization occurs in stage (I) as linear and branched oligomers are formed. Once these oligomers are formed, cyclization occurs relatively rapidly in stage (II) and then reaches a plateau as the oligomers combine to form a gel in stage (III). To observe the effects of ring size, the value of Cr_n at the gel point is compared as a function of κ for 3-ring and 4-ring cyclization in Figure 5. For $\kappa \leq 2$, the values of Cr_n of models with both ring sizes are small and almost identical. However, with increasing κ (especially when $\kappa \geq 5$), the number-average cycle ranks with four-membered rings are larger than those found with three-membered rings. For example, when $\kappa = 50$, the number-average cycle rank of four-membered rings is about 18.6 at $DP_w = 10{,}000$ (just after the gel point), while the corresponding value with three-membered rings is just about 10.8. This means that, on average, each molecule in the model with four-membered ring cyclization has at least seven more independent cycles at the gel point than each molecule in the model with three-membered ring cyclization. Naturally, this indicates that the molecular structure is more complex in the case of four-membered ring cyclization. This is because the variety and number of 3-bond blocks arrangements is much greater than 2-bond blocks. The reason for this result will be discussed later.

At each bimolecular reaction step, the total number of molecules decreases by one and the total number of cycles does not change. Therefore, the increment of number-average cycle rank due to a bimolecular reaction step is[11]

$$\Delta Cr_n = \frac{Cr_n}{N_{mol}} \tag{24}$$

where Cr_n is the number-average cycle rank and N_{mol} is the total number of molecules. At each cyclization reaction step, the total number of molecules remains the same and the total number of cycle rank is increased by one for the reactant molecule. Therefore, the incremental change in the number-average cycle rank due to a cyclization reaction is

$$\Delta Cr_n = \frac{1}{N_{mol}} \tag{25}$$

Comparing Eq. 24 with 25, it is easy to see that when Cr_n is larger than 1, ΔCr_n is larger for bimolecular reactions based on the same value of N_{mol}. Also, for both reactions, ΔCr_n is larger with smaller N_{mol}. When $\kappa = 50$, Table 1 showed that more bimolecular reactions occur in four-membered ring cyclization, so N_{mol} in the four-membered ring cyclization is smaller than that in the three-membered ring case after some steps. Therefore, the Cr_n values with four-membered rings are much larger than those with three-membered rings (as seen in Figure 5).

Ring involvement

Another measure of the average level of cyclization in the population of oligomers is ring involvement,[49] which is defined as the average number of independent rings in which a silicon site is involved. Ring involvement is 0 for every site in the beginning of the DMC simulation. Since one new independent ring is formed after each cyclization reaction, and each ring has four sites, ring involvement (I) is increased by

$$\Delta I = \frac{4}{N} \tag{26}$$

Supporting Information Figure S3 shows the ring involvement of four-membered rings as a function of conversion with varying κ. The curves have the same tendencies for simulations with three-[11] and four-membered rings: ring involvement increases with increasing conversion for all cases. With larger value of κ, the value of ring involvement at the gel point is higher. Figure 6 compares the values of I at the gel point for three- and four-membered ring cyclization. In cases corresponding to high gel conversion, for example, when $\kappa = 50$, ring involvement approaches 4 at the gel point (Figure 6). Thus, multiple rings per silica site (representing the formation of cage-like intermediates) are formed before gelation. For $\kappa \geq 5$, the ring involvement of four-membered rings cyclization is larger as that of three-

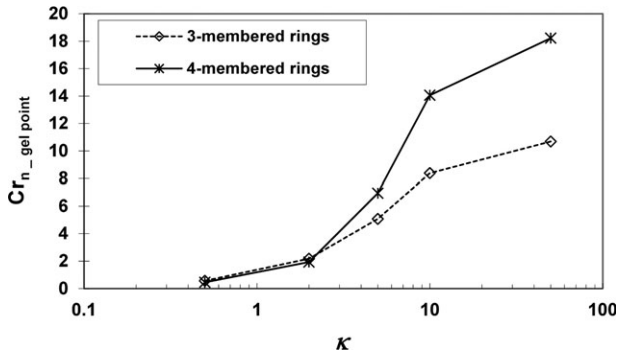

Figure 5. Number-average cycle rank at the gel point as a function of κ for DMC models with three- and four-membered rings.For all calculations, *Bi* = 1000, *Da* = 60, and h_{p0} = 0.8.

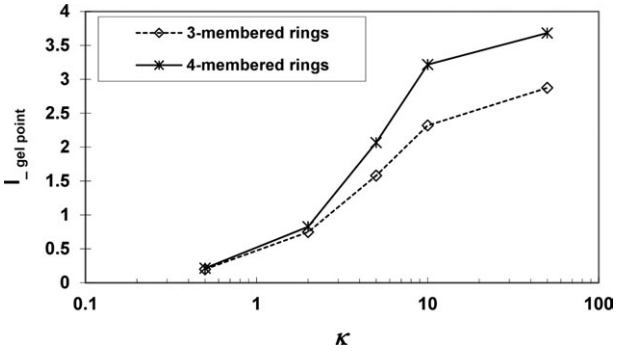

Figure 6. Ring involvement at the gel point as a function of κ for DMC simulations with three- or four-membered rings.

In both cases, $Bi = 1000$, $Da = 60$, and $h_{p0} = 0.8$.

membered ring cyclization. Therefore, a silica site is involved in more independent rings in the four-membered ring cyclization case than in the three-membered case. This is consistent with the earlier observation that the molecular structure is more complex with four-membered ring cyclization.

Gelation regime map

Two important dimensionless parameters, *Bi* and *Da,* are used in our multiscale model to summarize the competition between mass transfer (drying) and reaction (gelation) in the drying process of the sol-gel silica film. In all of the discussion above, arbitrary values of *Bi* and *Da* were used for all calculations, and the focus was on the effects of cyclization parameter. However, these results can be placed into context using gelation regime maps, as we did in our previous papers.[10,11] In the gelation regime map, there are three types of qualitative phenomena represented: drying before gelation, gelation before drying and literal skinning.[60] These are defined based on time-to-dry values (the time at which the average $C_1 = 0.01C_{1,0}$) and gelation times at the top and bottom of the film and, thus, give a global picture of the state of the film predicted by the multiscale DMC/continuum

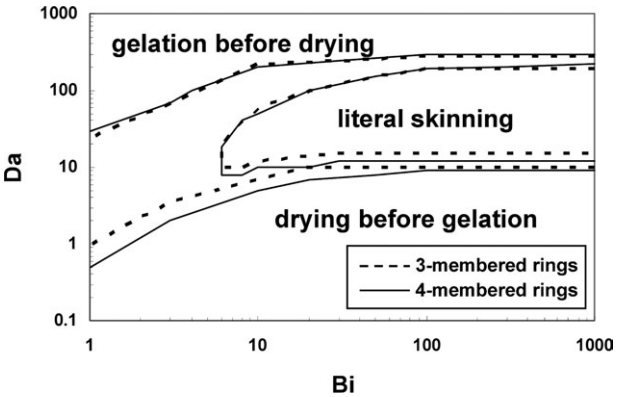

Figure 7. Gelation regime map with unlimited four-membered ring cyclization (solid curves) or three-membered ring cyclization (dashed curves) calculated with $\kappa = 5$.

The boundaries were derived by averaging drying times and gelation times at the base and surface of films using five replicate calculations.

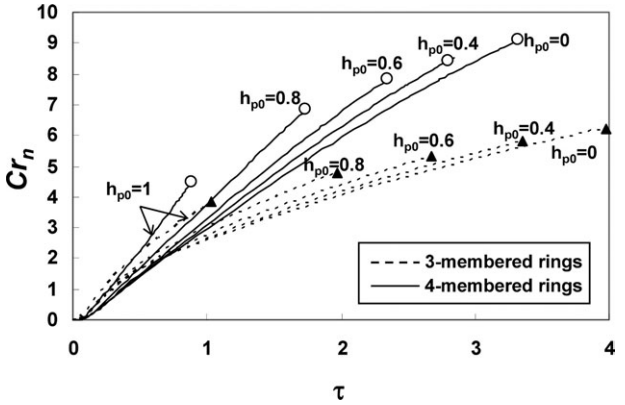

Figure 8. Number-average cycle rank as a function of dimensionless time with different initial particle positions for four-membered ring cyclization (solid curves) and three-membered ring cyclization (dashed curves).

For all simulations, $Bi = 1000$, $Da = 60$, and $\kappa = 5$. The plotted circles and triangles represent gel points.

model. As defined by Cairncross et al., literal skinning means that the difference between gel times at the base and surface of the film exceeds 10% of the drying time.[60] Figure 7 shows the gelation regime map for simulations with unlimited three- and four-membered ring cyclization and with a fixed value of $\kappa = 5$. For four-membered rings, this is an experimentally relevant value of κ. For the cases where Ng and McCormick were able to estimate $k_{4c(1,1)}$ and k_{11} of acid-catalyzed tetraethyl orthosilicate sol-gel solutions, the average ratio of the two has a value of about 5.5 mol/L.[22] Therefore, if an as-deposited sol has a concentration close to $[Si]_0 = 1$ mol/L, this gives a value for a realistic sol-gel silica solution of $\kappa \sim 5$. Also in terms of the modeling, this value is interesting to study because it represents the conditions with greatest sensitivity of gel conversion difference between film surface and base (and therefore gel structure) to concentration. On Figure 7, the gelation regime map boundaries of a multiscale model with three-membered rings are also plotted. They are very similar and almost overlap, but the literal skinning region is subtly expanded in the four-member ring case.

As discussed above, one of the advantages of our multiscale model is that it allows us to probe the microstructural implications of macroscopic transport processes. One of the unique insights it offers is insight into structural gradients that can form as a result of concentration gradients present during literal skinning. An example of the effect of three- and four-membered ring cyclization on literal skinning is shown in Figure 8. This figure shows number-average cycle rank as a function of dimensionless time for different initial particle positions. The first thing that we can notice from this figure is that according to the gel points (circles or triangles) on the graph, the film gels much faster at the surface ($h_{p0} = 1$) than inside the film. That means there is a time lag of gelation between the film surface and base. Such time lags are characteristic of literal skinning and are seen in all gelling/drying systems under the right conditions. However, a new feature is also revealed: the gel points on the curves indicate what extent of number-average cycle rank can be reached before gelation for different initial sol particle

position. Figure 8 clearly shows that the number-average cycle rank at the gel point inside the film is twice as large as it is at the film surface when four-membered rings are allowed. Therefore, there is a molecular structure gradient inside the film. We compare this finding with the corresponding results for three-membered rings using the dashed curves in Figure 8. The values of number-average cycle rank at the gel point with four-membered rings are larger than the values with three-membered rings, and the gel times are also reduced with four-membered rings. The gradient in number-average cycle rank is also smaller for the model with three-membered rings; the interior of the film has only $\sim$ 60% more rings per molecule in Figure 8. Figure 9 also shows that the gradient of ring involvement at the gel point is larger for the four-membered ring case. Thus, at the same conditions (*Bi*, *Da* and κ), compared with a model having three-membered ring cyclization, the DMC/continuum model with four-membered ring cyclization shows faster gelation, a large number-average cycle rank, and a larger gradient of structure across a film with literal skinning.

Structure gradient map

As discussed above, direct measures of cyclization such as ring involvement and cycle rank increase as the cyclization tendency increases. Also, the conversion at gelation increases in a way that is correlated with cyclization. Therefore, a measure of the structure gradient in a film is the difference in gel conversion between the surface and base, $\Delta\alpha_{gel}$. Figure 10 compares structure gradient maps for the multiscale model performed with four- or three-membered ring cyclization and κ = 5, which is a contour plot of gel conversion difference vs. *Bi* and *Da*. The regions of *Bi* and *Da* with high values of $\Delta\alpha_{gel}$ coincide with the literal skinning region of the gelation regime map. Comparing Figure 10a with b, all the regions in Figure 10b move to much smaller values of *Bi* and *Da*, especially for the large $\Delta\alpha_{gel}$ value of 0.1. Therefore, structure gradients occur more easily in the model with four-membered rings than in the model with three-membered rings. This suggests that in the real films, where four-membered rings are the predominant species, drying under conditions of high *Bi* and *Da* is likely to lead to structure gradients where the top of the film has "skin" that gels quickly and has fewer cycles, while the interior of the film (near the base) is made up of cage-like precursors. The polymer network with fewer cycles is likely to be more elastic and tough, while a network made up weakly linked, rigid cages would be expected to be more brittle. This would be expected to exacerbate the problems encountered with defect formation due to skinning in sol-gel films. The best way to avoid this problem is most likely to push the conditions towards the "drying before gelation" drying regime, so that a uniform gel film without residual solvent forms.

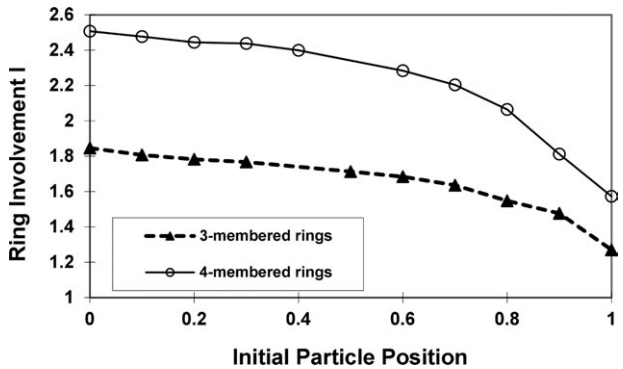

Figure 9. Ring involvement at the gel point as a function of initial particle position for a representative four- and three-membered ring cyclization literal skinning case: *Bi* = 1000, *Da* = 60, and κ = 5.

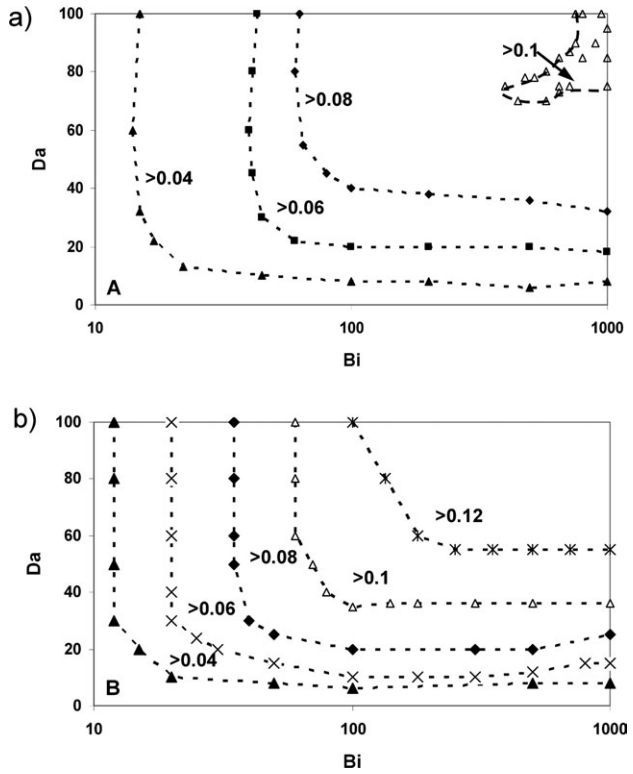

Figure 10. Structure gradient map for the (a) three-membered and (b) four-membered ring cyclization with κ = 5.

The contours were estimated by taking average values of five replicates at each condition to determine the difference in gel conversion at the top and bottom of the film. Dashed lines are the approximate contours of constant $\Delta\alpha_{gel}$.

Conclusions

The results of a multiscale model for the drying and curing process of sol-gel silica films with unlimited four-membered ring cyclization were presented. Two main links between the parts of the multiscale model are as follows: first, in the continuum model, the entire DMC simulation is treated as a particle of sol whose position and composition are tracked using a diffusion/evaporation finite difference calculation. The importance of this particle tracking is that the continuum model provides the total silicon concentration for the DMC model, and this thus serves as a spatially distributed "handshake" between the DMC and continuum calculations. The second "handshake" between the models is the time interval for each bond addition in the DMC simulation, which is used as the time interval for the finite difference calculation.

By comparing with our previous model of drying sol-gel films with unlimited three-membered ring cyclization, this

new model allowed us to comment on a more physically relevant type of cyclization. As in the previous model, the model with four-membered rings showed that the gel conversion increases as dimensionless cyclization tendency κ increases, and for reasonable values of κ, gel conversion meeting or exceeding the experimental value (82%) was observed. Calculations of the topological Wiener index clearly showed that cyclization shrinks the molecular size, including in extreme cases the formation of cage-like precursors that remain compact until the gel point.

For $\kappa \geq 5$, on average, each molecule in the new model with four-membered rings has more independent cycles than each molecule in the former model with three-membered rings, indicating that the molecular structure is more complex in the four-membered ring case. A gelation regime map shows the competition between mass transfer (drying) and reaction (gelation) in the coating process of the sol-gel silica films. The gelation regime maps of models with four-membered rings and with three-membered rings were found to be very similar and almost overlapped; the only difference is that the literal skinning region of is a very slightly expanded with four-membered rings.

The relationships between measures of cyclization (ring involvement and number-averaged cycle rank) and conversion, time and initial particle position were investigated. The simulations showed that cage-like intermediates form before gelation when the gel conversion is high (with large κ). The number-average cycle rank and the ring involvement at gel conversion inside the film are much larger than that at the surface in many experimentally relevant conditions, so that there is a molecular structure gradient inside the film. At the same conditions (Bi, Da, and κ), compared with the three-membered ring case, four-membered ring cyclization causes gels to form more quickly and produces gels with more rings per molecule. This gives rise to larger structure gradients in the films with four-membered rings than those found in films with three-membered rings. The formation of gel structure gradients would be expected to exacerbate defect formation due to literal skinning.

While its development has been complex, this multiscale model represents a first step to understanding the complete coating process of sol-gel silica. The inclusion of unlimited four-membered ring cyclization will give more accurate and relevant predictions than our previous models. Still, this model can be improved in several ways in the future. For example, transport properties were assumed to be constant during polymerization. The multiscale model provides the opportunity for more ''handshaking'' between the model components to improve this situation. One way of doing this it to utilize the Wiener index with diffusivity correlations to provide a more physically relevant self-consistent continuum/DMC result in the future. In addition, some limitations may need to be added for the cyclization reactions, because realistic molecular structures need to be constrained by the actual bond angles and energies of the oligomers. Although four-membered rings are the dominant units, there are still some three-membered rings found in the experiments. Therefore, a more comprehensive model would combine three- and four-membered ring cyclization and would include reversibility of cyclization. This, obviously, is a substantial challenge even with available computational resources, but these are challenges that can be overcome in future developments.

Acknowledgments

This report is based on work supported by the U.S. Department of Energy under grant numbers DE-FG02-03ER46033 and DE-FG02-07ER46375.

Notation

Bi = Biot number
${}^{n}B_{ij}$ = n-bond block with ends connectivity i, j
${}^{3}B_{ij}$ = 3-bond block with ends connectivity i, j
C = concentration
C_0 = reference concentration
C_{Si} = total silicon site concentration (at the particle position)
c = dimensionless concentration
c_i^s = dimensionless concentration at the surface of the solution
Cr_i = the cycle rank of molecule i
Cr_n = the number-average cycle rank
Cr_w = the weight-average cycle rank
D = diffusion coefficient
Da = Damköhler number
DP_w = the weight-average degree of polymerization
f = the functionality of the monomer
h = the dimensionless thickness of the film at time t
$H(t)$ = the thickness of the film at time t
h_{p0} = the initial particle position inside the film as a fraction of the initial film thickness
H_0 = the initial thickness of the film
I = ring involvement
k_{ij} = rate coefficient of bimolecular polycondensation
$k_{4c(i,j)}$ = rate coefficient of four-membered rings cyclization
k_g = mass-transfer coefficient of solvent in the vapor-phase
m = the degree of polymerization of a molecule
MW_i = molecular weight of molecule i
N = the total numbers of sites/monomers considered in DMC method
n = the degree of polymerization of a molecule
N_{mol} = the total numbers of molecules in MC method
P_1 = the solvent vapor pressure
P_t = the total pressure
Q_i = tetrafunctional silicon site with i siloxane bonds
$[Q_i]$ = the concentration of Q_i
r = the random number from (0, 1)
R_{ij}^{bimol} = bimolecular reaction
${}^{4}R_{ij}^{cyc}$ = four-membered ring cyclization reaction
S_b = the steps of bimolecular reactions
S_c = the steps of cyclization reactions
S_t = the total MC steps at the gel point
$[Si]_0$ = initial monomer concentration
t = time
Δt = time interval calculated by MC method
v^s = the free surface velocity
$\hat{V}$ = molar volume
W = Wiener index
W_i = Wiener index of molecule i
W_n = number-average Wiener index
$W_{n,lin}$ = number-average Wiener index of linear molecules
W_{new} = the increment of Wiener index after a reaction
xm = the molar fraction of solvent in solution
y_1^s = the molar fraction of solvent just above the film surface in the gas phase
y_1^∞ = the molar fraction of solvent far away in the gas phase
z = distance from the bottom
α = siloxane bond conversion
$\Delta\alpha_{gel}$ = the gel conversion difference between the film surface and base
η = dimensionless distance from the bottom
κ = cyclization tendency
τ = dimensionless time
χ = hydrolysis extent

Subscripts

With C:
1 = solvent
2 = total silicon

Literature Cited

1. Sanchez C, Boissiere C, Grosso D, Laberty C, Nicole L. Design, synthesis, and properties of inorganic and hybrid thin films having periodically organized nanoporosity. *Chem Mater*. 2008;20:715–720.
2. Guliants VV, Carreon MA, Lin YS. Ordered mesoporous and macroporous inorganic films and membranes. *J Membr Sci*. 2004;235:53–72.
3. Brinker CJ, Dunphy DR. Morphological control of surfactant-templated metal oxide films. *Curr Opin Colloid Interface Sci*. 2006;11:126–132.
4. Innocenzi P, Malfatti L, Soler-Illia G. Hierarchical mesoporous films: from self-assembly to porosity with different length scales. *Chem Mater*. 2011;23:2501–2509.
5. Innocenzi P, Malfatti L, Kldchob T, Falcaro P. Order-disorder in self-assembled mesostructured silica films: a concepts review. *Chem Mater*. 2009;21:2555–2564.
6. Dušková-Smrcková M, Dušek K. Processes and states during polymer film formation by simultaneous crosslinking and solvent evaporation. *J Mater Sci*. 2002;37:4733–4741.
7. Doshi DA, Gibaud A, Liu NG, Sturmayr D, Malanoski AP, Dunphy DR, Chen HJ, Narayanan S, MacPhee A, Wang J, Reed ST, Hurd AJ, van Swol F, Brinker CJ. In-situ X-ray scattering study of continuous silica-surfactant self-assembly during steady-state dip coating. *J Phys Chem B*. 2003;107:7683–7688.
8. Innocenzi P, Malfatti L, Kidchob T, Costacurta S, Falcaro P, Piccinini M, Marcelli A, Morini P, Sali D, Amenitsch H. Time-resolved simultaneous detection of structural and chemical changes during self-assembly of mesostructured films. *J Phys Chem C*. 2007;111:5345–5350.
9. Grosso D, Cagnol F, Soler-Illia G, Crepaldi EL, Amenitsch H, Brunet-Bruneau A, Bourgeois A, Sanchez C. Fundamentals of mesostructuring through evaporation-induced self-assembly. *Adv Funct Mater*. 2004;14:309–322.
10. Li X, Rankin SE. Multiscale dynamic Monte Carlo/continuum model of drying and nonideal polycondensation in sol-gel silica films. *AIChE J*. 2010;56:2946–2956.
11. Li X, Rankin SE. Influence of unlimited 3-membered ring cyclization on a multiscale dynamic Monte Carlo/continuum model of drying and curing in sol-gel silica films. *Chem Eng Sci*. 2011;66:1015–1026.
12. West JK, Zhu BF, Cheng YC, Hench LL. Quantum chemistry of sol-gel silica clusters. *J Non-Cryst Solids*. 1990;121:51–55.
13. Tang A, Xu R, Li S, An Y. Characterisation of polymeic reaction in silicic acid solution: intramolecular cyclization. *J Mater Chem*. 1993;3:893–896.
14. Sanchez J, McCormick AV. Intramolecular vs. intermolecular condensation rates in the acidic polymerization of octaethoxytrisiloxane. *J Non-Cryst Solids*. 1994;167:289–294.
15. Ng LV, Thompson P, Sanchez J, Macosko CW, McCormick AV. Formation of cagelike intermediates from nonrandom cyclization during acid-catalyzed sol-gel polymerization of tetraethyl orthosilicate. *Macromolecules*. 1995;28:6471–6476.
16. Vainrub A, Devreux F, Boilot JP, Chaput F, Sarkar M. Sol-gel polymerization in alkoxysilanes: 29Si NMR study and simulation of chemical kinetics. *Mater Sci Eng B*. 1996;B37:197–200.
17. Malier L, Boilot JP, Chaput F, Devreux F. Nuclear-magnetic-resonance study of silica gelation kinetics. *Phys Rev A*. 1992;46:959–962.
18. Bailey JK, Macosko CW, Mecartney ML. Modeling the gelation of silicon alkoxides. *J Non-Cryst Solids*. 1990;125:208–223.
19. Earley CW. A quantum mechanical investigation of silsesquioxane cages. *J Phys Chem*. 1994;98:8693–8698.
20. Brunet F. Polymerization reactions in methyltriethoxysilane studied through ^{29}Si NMR with polarization transfer. *J Non-Cryst Solids*. 1998;231:58–77.
21. Kelts LW, Armstrong NJ. A silicon-29 NMR study of the structural intermediates in low pH sol-gel reactions. *J Mater Res*. 1989;4:423–433.
22. Ng LV, McCormick AV. Acidic sol-gel polymerization of TEOS: effect of solution composition on cyclization and bimolecular condensation rates. *J Phys Chem*. 1996;100:12517–12531.
23. Rankin SE, Macosko CW, McCormick AV. Sol-gel polycondensation kinetic modeling: methylethoxysilanes. *AIChE J*. 1998;44:1141–1156.
24. Van Beek JJ, Seykens D, Jansen JBH. Silicon-29 NMR monitoring and kinetic modeling of an acid-catalyzed TMOS sol-gel system with molar water/silicon = 8. *J Non-Cryst Solids*. 1992;146:111–120.
25. Capozzi CA, Pye LD, Condrate RA Sr. Vibrational spectral/structural changes from the hydrolysis/polycondensation of methyl-modified silicates. I. Comparisons for single monomer condensates. *Mater Lett*. 1992;15:130–136.
26. Tallant DR, Bunker BC, Brinker CJ, Balfe CA. Raman spectra of rings in silicate materials. *Mater Res Soc Symp Proc*. 1986;73:261–267.
27. Kamiya K, Dohkai T, Wada M, Hashimoto T, Matsuoka J, Nasu H. X-ray diffraction of silica gels made by sol-gel method under different conditions. *J Non-Cryst Solids*. 1998;240:202–211.
28. Wada M, Kamiya K, Nasu H, Matsuoka J, Yoko T, Fukunaga T, Misawa M. Structure analysis of sol-gel-derived silica gels by neutron diffraction. *J Non-Cryst Solids*. 1992;149:203–208.
29. Klemperer WG, Mainz VV, Ramamurthi SD, Rosenberg FS. Structural characterization of polysilicate intermediates formed during sol-gel polymerization. *Mater Res Soc Symp Proc*. 1988;121:15–24.
30. Rao NZ, Gelb LD. Molecular dynamics simulations of the polymerization of aqueous silicic acid and analysis of the effects of concentration on silica polymorph distributions, growth mechanisms, and reaction kinetics. *J Phys Chem B*. 2004;108:12418–12428.
31. Schumacher C, Gonzalez J, Wright PA, Seaton NA. Generation of atomistic models of periodic mesoporous silica by kinetic Monte Carlo simulation of the synthesis of the material. *J Phys Chem B*. 2006;110:319–333.
32. Malani A, Auerbach SM, Monson PA. Probing the mechanism of silica polymerization at ambient temperatures using Monte Carlo simulations. *J Phys Chem Lett*. 2010;1:3219–3224.
33. Campo FA, Murillo JSR, Barbero EJ. Aggregation model for the gelation of a sol starting from the processing conditions. *J Non-Cryst Solids*. 2011;357:2046–2053.
34. Zhang XQ, Trinh TT, van Santen RA, Jansen APJ. Mechanism of the initial stage of silicate oligomerization. *J Am Chem Soc*. 2011;133:6613–6625.
35. Šomvársky J, Dušek K. Kinetic monte-carlo simulation of network formation .1. Simulation method. *Polym Bull*. 1994;33:369–376.
36. Šomvársky J, Dušek K. Kinetic monte-carlo simulation of network formation .2. Effect of system size. *Polym Bull*. 1994;33:377–384.
37. Majumder D, Broadbelt LJ. A multiscale scheme for modeling catalytic flow reactors. *AIChE J*. 2006;52:4214–4228.
38. Cheimarios N, Kokkoris G, Boudouvis AG. Multiscale modeling in chemical vapor deposition processes: coupling reactor scale with feature scale computations. *Chem Eng Sci*. 2010;65:5018–5028.
39. Dollet A. Multiscale modeling of CVD film growth—a review of recent works. *Surf Coat Technol*. 2004;177:245–251.
40. Vlachos DG. Multiscale integration hybrid algorithms for homogeneous-heterogeneous reactors. *AIChE J*. 1997;43:3031–3041.
41. Braatz RD, Alkire RC, Seebauer EG, Drews TO, Rusli E, Karulkar M, Xue F, Qin Y, Jung MYL, Gunawan R. A multiscale systems approach to microelectronic processes. *Comput Chem Eng*. 2006;30:1643–1656.
42. Cavallotti C, Di Stanislao M, Moscatelli D, Veneroni A. Materials computation towards technological impact: the multiscale approach to thin films deposition. *Electrochim Acta*. 2005;50:4566–4575.
43. Sanchez J, Rankin SE, McCormick AV. ^{29}Si NMR kinetic study of tetraethoxysilane and ethyl-substituted ethoxysilane polymerization in acidic conditions. *Ind Eng Chem Res*. 1996;35:117–129.
44. Rankin SE, Šefčík J, McCormick AV. Similarities in the hydrolysis pseudoequilibrium behavior of methyl-substituted ethoxysilanes. *Ind Eng Chem Res*. 1999;38:3191–3198.
45. Rankin SE, McCormick AV. Hydrolysis pseudoequilibrium: challenges and opportunities to sol-gel silicate kinetics. *Chem Eng Sci*. 2000;55:1955–1967.
46. Assink RA, Kay BD. The chemical kinetics of silicate sol-gels: functional group kinetics of tetraethoxysilane. *Colloids Surf A*. 1993;74:1–5.
47. Assink RA, Kay BD. Sol-gel kinetics. I. Functional group kinetics. *J Non-Cryst Solids*. 1988;99:359–370.
48. Pouxviel JC, Boilot JP. Kinetic simulations and mechanisms of the sol-gel polymerization. *J Non-Cryst Solids*. 1987;94:374–386.
49. Rankin SE, Kasehagen LJ, McCormick AV, Macosko CW. Dynamic Monte Carlo simulation of gelation with extensive cyclization. *Macromolecules*. 2000;33:7639–7648.
50. Kasehagen LJ, Rankin SE, McCormick AV, Macosko CW. Modeling of first shell substitution effects and preferred cyclization in sol-gel polymerization. *Macromolecules*. 1997;30:3921–3929.
51. Gillespie DT. A general method for numerically simulating the stochastic time evolution of coupled chemical reactions. *J Comput Phys*. 1976;22:403–434.
52. Schilstra MJ, Martin SR. *Simple stochastic simulation*. In: Michael LJ, Ludwig B, editors. *Methods in Enzymology*. San Diego, CA: Academic Press, Vol.476, 2009:381–409.
53. Chatterjee A, Vlachos DG. An overview of spatial microscopic and accelerated kinetic Monte Carlo methods. *J Comp-Aided Mater Design*. 2007;14:253–308.

54. Fichthorn KA, Weinberg WH. Theoretical foundations of dynamical Monte Carlo simulations. *J Chem Phys*. 1991;95:1090–1096.
55. Wiener H. Structural determination of paraffin boiling points. *J Am Chem Soc*. 1947;69:17–20.
56. Nitta KH. A topological approach to statistics and dynamics of chain molecules. *J Chem Phys*. 1994;101:4222–4228.
57. Sarmoria C, Miller DR. Spanning-tree models for Af homopolymerizations with intramolecular reactions. *Comp Theor Polym Sci*. 2001;11:113–127.
58. Guerrier B, Bouchard C, Allain C, Bénard C. Drying kinetics of polymer films. *AIChE J*. 1998;44:791–798.
59. Crank J. *Free and Moving Boundary Problems*. Oxford: Clarendon Press, 1988.
60. Cairncross RA, Francis LF, Scriven LE. Predicting drying in coatings that react and gel: drying regime maps. *AIChE J*. 1996;42:55–67.

Manuscript received Mar. 14, 2012, and revision received May 11, 2012.